Broadband performance of TPF's High-Contrast Imaging Testbed: Modeling and simulations

Erkin Sidick*, Andreas C. Kuhnert, and John T. Trauger
Jet Propulsion Laboratory, California Institute of Technology, 4800 Oak Grove Drive, Pasadena, CA, USA 91109

ABSTRACT

The broadband performance of the high-contrast imaging testbed (HCIT) at JPL is investigated through optical modeling and simulations. The analytical tool is an optical simulation algorithm developed by combining the HCIT's optical model with a speckle-nulling algorithm that operates directly on coronagraphic images, an algorithm identical to the one currently being used on the HCIT to actively suppress scattered light via a deformable mirror. It is capable of performing full three-dimensional end-to-end near-field diffraction analysis on the HCIT's optical system. By conducting speckle-nulling optimization, we clarify the HCIT's capability and limitations in terms of its broadband contrast performance under various realistic conditions. Considered cases include non-ideal occulting masks, such as a mask with optical density and wavelength dependent parasitic phase-delay errors (i.e., a not band-limited occulting mask) and the one with an optical-density profile corresponding to a measured, non-standard profile, as well as the independently measured phase errors of all optics. Most of the information gathered on the HCIT's optical components through measurement and characterization over the last several years at JPL has been used in this analysis to make the predictions as accurate as possible. The best contrast values predicted so far by our simulations obtainable on the HCIT illuminated with a broadband light having a bandwidth of 80nm and centered at 800nm wavelength are C_m=1.1x10^{-8} (mean) and C_4=4.9x10^{-8} (at 4λ/D), respectively. In this paper we report our preliminary findings about the broadband light performance of the HCIT.

Keywords: TPF, integrated modeling, speckle-nulling, high-contrast coronagraph

1. INTRODUCTION

High-contrast imaging testbed (HCIT) at JPL is Terrestrial Planet Finder (TPF) Coronagraph's primary platform for experimentation [1-2]. It is used to provide laboratory validation of key technologies as well as demonstration of a flight-traceable approach to implementation. In order to validate the HCIT's performance through modeling and error budget analysis, we have implemented an optical simulation algorithm by combining the HCIT's optical model [3] with a speckle-nulling algorithm. This simulation algorithm uses MACOS (Modeling and Analysis for Controlled Optical Systems) [4], a versatile optical modeling tool developed at JPL and used in many flight projects. Hence it is capable of performing full near-field diffraction analysis on the HCIT's optical system. Such a diffraction analysis is required to evaluate the HCIT's performance in terms of design tolerances and based on its ultimate metric—the contrast ratio. MACOS also allows seamless interfacing with structural and thermal models, thus eventually enabling us to create fully integrated optical/structural/thermal models to evaluate the dynamic effects of disturbances on the overall performance of the HCIT.

Recently, we reported our modeling and simulation results on the monochromatic wavelength performance of the HCIT [5]. In that study, our modeling predicted within a "half dark hole" a monochromatic Mean Contrast of C_m=2x10^{-11} and a contrast at an angular separation 4λ/D of C_4=5x10^{-11}, in contrast to the measured results of C_m~6x10^{-10} and C_4~8x10^{-10}, respectively. One of the remaining HCIT milestones is to achieve a broadband contrast less than C_4=1x10^{-9}. Here, the broadband contrast is defined as the one obtained with a broadband light source centered at 800nm wavelength and having a bandwidth of ±5%, or Δλ=80nm. Work is currently underway to optimize the HCIT for such a broadband operation. To assist this experimental development and to understand the HCIT's capabilities and limitations, we have carried out optical modeling and simulations on the broadband performance of the HCIT's optical system. The structural design of the optical system as well as the parameters of various optical elements used in the analysis are

*Erkin.Sidick@jpl.nasa.gov; Phone 1 818 393-7585; Fax 1 818 393-9471; www.jpl.nasa.gov

identical to those of the implemented HCIT. One of the key goals of this modeling is to find an effective method for broadband speckle-nulling. Another important goal is to create an error budget table for HCIT. In this paper, we report our preliminary findings on the broadband contrast performance of the HCIT. The focus of this paper is to baseline the broadband performance of the HCIT in its current state. The investigation of the HCIT through modeling and simulations is an on-going effort and we will continue our work on optimizing the optical design parameters for broadband operation as well as on finding an effective method for broadband speckle-nulling optimization.

2. OPTICAL SYSTEM AND COMPONENTS

The MACOS optical model realistically mimics the HCIT. The centerpiece of the HCIT is a 5x7 foot optical table, on which are installed the coronagraph elements as schematically shown in Figure 1. The whole optical table sits in a thermally controlled vacuum tank evacuated with a scroll pump to 10 milli-Torr or better. The tank provides the desired environment, including vibration isolation, atmospheric turbulence isolation and sub-Kelvin thermal stability. An artificial starlight is created by a 5μm pinhole illuminated by an optical fiber. Various light sources can be fed into the other end of the fiber outside the vacuum tank, such as a narrow band laser beam or a broadband light source with 20% or more bandwidth. An off-axis parabolic mirror (OAP1) collimates the light from the pinhole and directs it to a high-density deformable mirror (DM), which performs the wavefront control. The aperture mask on the DM defines the system pupil of the HCIT. After the DM, the collimated light is re-imaged onto the focal plane of the occulting mask by OAP2 and a flat mirror (FM1). The occulting mask attenuates the starlight, and almost has no effect on the light of a planet if present. The "back-end" of the system, from the occulting mask to the back focus plane, supports experimentation with diverse coronagraph configurations and apodizations. This optical setup corresponds to a classical Lyot coronagraph: an occulting mask at the highly-corrected focal plane plus a Lyot mask at the subsequent pupil plane.

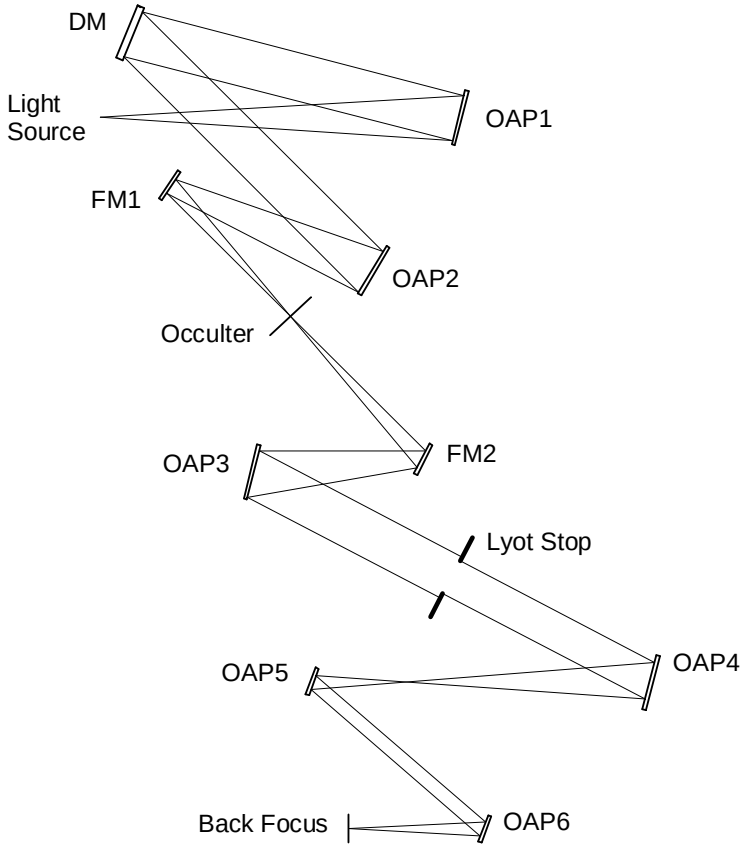

Figure 1. Schematic diagram of the High Contrast Imaging Testbed layout. The light source ("starlight") is a 5μm pinhole illuminated by an optical fiber, and a CCD science camera is located at the back focal plane for detecting the image of the "starlight".

A flat mirror (FM2) and OAP3 re-collimate the light passing through the occulter mask and form a same-size sharp image of the DM pupil at the Lyot plane. A Lyot stop blocks the ring-like residual light diffracted off the occulter mask while letting most of the planet light through. After OAP4 forms an image from the remaining stellar and planet lights, it is then magnified (M ≈3) by the OPA5-OAP6 pair for proper sampling on the CCD science camera located at the back focal plane. On the testbed, the wavefront control software takes the starlight image captured by the CCD camera as an input, finds a new set of DM control commands from it, then updates the DM settings with the new set of control commands.

We use a system aperture diameter D=30mm throughout our analysis. The characteristics and the physical parameters of various optical components used in this study are identical to those described in detail in Ref. 5. That is, the amplitude drooping of the illuminating beam exhibited at the exit pupil, the phase errors of the various optics, and the Lyot Stop parameter ε=0.40 are still the same. Therefore, they are not repeated here. There is some new information about the occulting mask used in the current investigation, thus it will be described separately in the following sub-section.

2.1 Occulting Mask

Phase versus OD

One of the occulting masks implemented on the HCIT is a gray-scale pattern written on a high-energy e-beam sensitive (HEBS) glass with the high e-beam lithography facility at JPL [6]. The intended target of the occulter has a linear-Sinc^2 intensity profile [7] with a width of w=141.9μm or w=144.0μm given by

$$T(x) = \left[1 - \left(\frac{\sin(\pi x / w)}{(\pi x / w)} \right)^2 \right]^2 . \qquad (1)$$

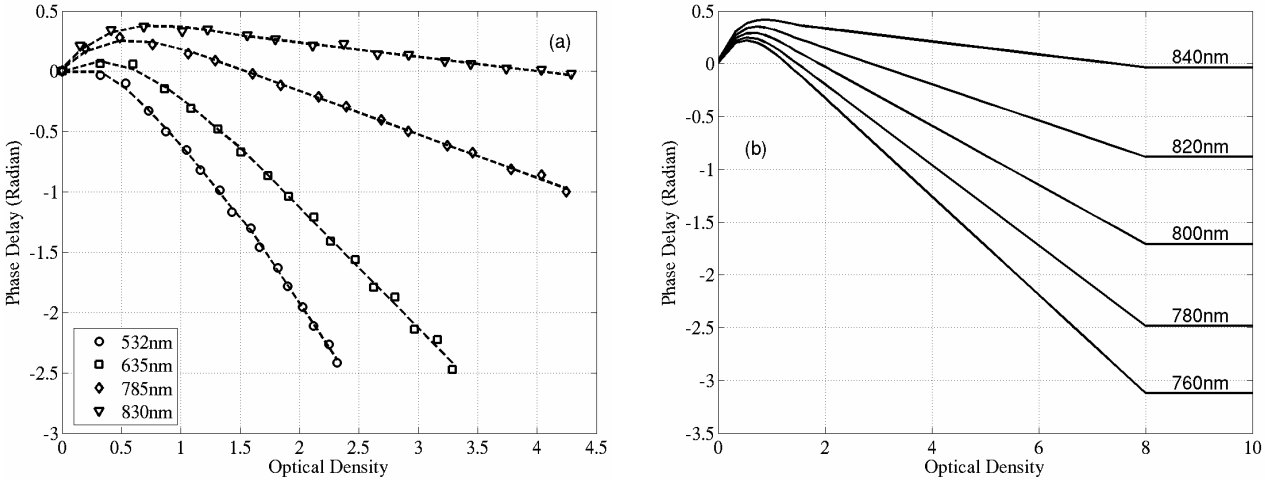

Figure 2. Phase delay as a function of OD with wavelength as a parameter. (a) Measured data of a HEBS glass (symbols, Ref. 8) and the corresponding curves obtained from an analytical curve-fitting expression; (b) Phase-delay versus OD curves at other wavelengths of interest obtained from an analytical curve-fitting expression.

A group at JPL has characterized the fundamental optical properties of this kind of occulting masks through measurement of the optical density (OD), the phase delay and the optical constants of the mask material and/or through direct measurement of the fabricated occulting masks [6, 8]. A set of phase versus OD data obtained through such measurement and used in the current analysis are shown in Fig. 2(a) with the different symbols representing the different wavelengths. We have developed an analytical model for this type of phase-OD relationship $\phi=\phi(OD,\lambda)$, and used it to obtain the occulter phase information at different wavelengths and at regions where OD > 4.5. Here λ is the wavelength. The dashed-curves in Fig. 2(a) and all of the curves in Fig. 2(b) were obtained using this analytical model. The

measured data in Fig. 2(a) are similar to the one presented in Fig. 11 of Ref. 8, and are re-plotted here as a validation of our analytical model.

As we can see from Fig. 2, there are 3 distinctive regions in each $\phi(OD,\lambda)$ curve: A nonlinear region at $OD < 1.5$, a linear region at $1.5 \le OD < 8$, and a truncated region at $OD \ge 8$. The measured data have been limited to $OD < 4.5$, and our analytical model represents the measured data fairly well in the first 2 regions. It has not been possible for our group at JPL to measure OD values at the OD=8 level and beyond, therefore, we introduced the truncated region in Fig. 2(b) as a guess to fill the empty region at $OD > 8$.

OD and Phase Profiles

Figure 3 shows the OD and phase profiles of an occulter fabricated at JPL. In this figure, the OD curve in Fig. 3(a) represents the measured data, and the phase profiles in the remaining two parts of this figure are obtained using our analytical model for $\phi=\phi(OD,\lambda)$. The OD values of this type of occulting mask changes slightly with wavelength [8], but such an effect is not taken into account in this study.

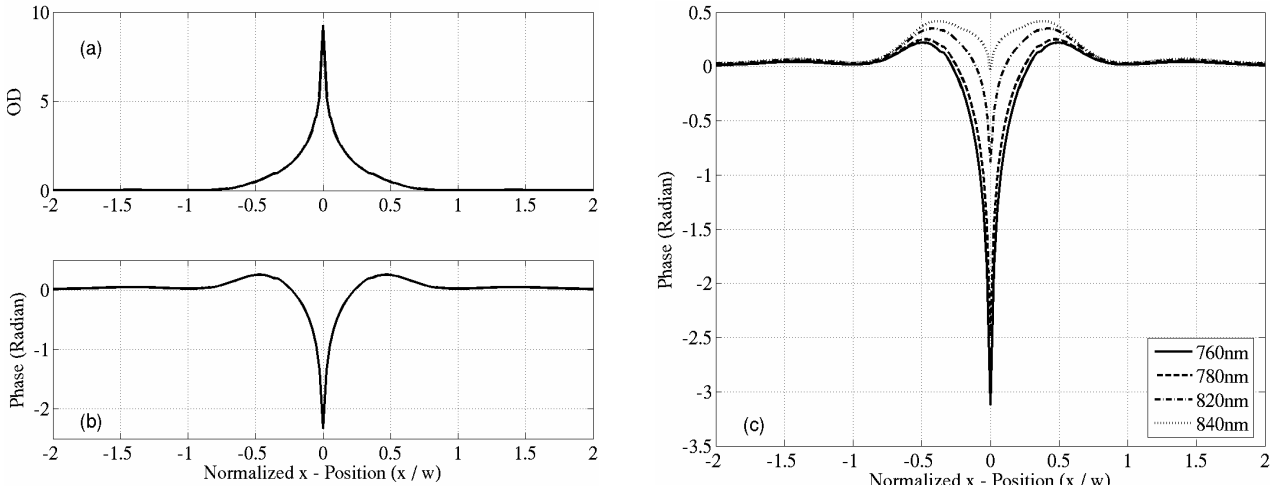

Figure 3. OD and phase profiles of a linear-Sinc^2 occulting mask. (a) OD profiles measured at λ=785nm; (b) Phase-delay profiles corresponding to the OD profile in part (a); (c) Phase profiles at various wavelengths obtained from the analytical model for $\phi=\phi(OD,\lambda)$.

There are two aspects of the above data that need to be explained. (i) The OD profile measurement was carried out on an occulting mask with w=141.9μm made with a Canyon Materials' HEBS glass Formulation A. The experimental setup for measuring such OD profiles is described in reference [6]. The particular OD data shown here were measured at a wavelength of λ=785 nm. This setup has a noise floor of OD~3. It was found that the measured OD profile starts to deviate from the target at $OD > 1$, and such deviation becomes significant at OD~3 and above. Therefore, the measured OD values in Fig. 3(a) corresponding to $OD > 1$ have been obtained by fitting a model of the form given by Eqn. 1 to the measured data at $OD \le 1$. Obtained occulting mask width of this fit is w=144.0μm. A linear-Sinc^2 occulter currently being used on the HCIT also has w=144.0μm. (ii) The phase measurement was carried out with a HEBS glass Formulation B, darkened using high electron beam at selected wavelengths of 532, 635, 785 and 830 nm. Details of this measurement are given in Ref. 8. Our analytical model for $\phi=\phi(OD,\lambda)$ is based on these measured data as explained above. That is, the phase curves in Fig. 3 are an estimate that is based on the measured data of a different type of HEBS material. A linear-Sinc^2 occulting mask being used on the testbed was made of an HEBS glass that is different from both Formulations A and B. But in our analysis we always used occulting mask phase profiles that were estimated with the above approach. That is, the occulting mask phase profiles used in our analysis are not identical to those of the actual devices, but we expect they are good estimates of what we really have on our testbed.

Measured (Polyfit) versus Design (Sinc^2)

The measured OD profile of a linear-Sinc^2 occulting mask was found to be slightly different from the target due to some fabrication and/or measurement error. In order to understand the impact of such errors in the occulting mask OD profile on the HCIT's performance, we compared the contrast results obtained with the above measured OD profile with those obtained with an ideal linear-Sinc^2 occulting mask, and found, to our surprise, that the measured (and "distorted") OD profile works better as compared to the target OD profile, as described in Ref. 5. In order to understand what is the cause contributing to this improved performance of the HCIT, we examined extensively the various factors associated with the measured OD profile. These factors include: (1) Occulter width parameter w, (2) the damped (or smoothed) ripples near the center of the occulting mask OD profile (Ref. 5), (3) noise spikes in the measured occulter OD profile data, and (4) the non-Sinc^2 shape of the OD curve in the $0.3 < |x/w| \leq 1$ regions, see Fig. 4(a). We found as a result of this investigation that the last factor, that is, the non-Sinc^2 shape of the OD curve in the $0.3 < |x/w| \leq 1$ regions, are responsible for the improvement in the HCIT's contrast performance. This is one of the significant findings of this study. That is, when the occulting mask has a parasitic phase (or is not band-limited), the standard Sinc^2 OD profile is not the best choice for a Lyot coronagraph. The slight discontinuity in the dashed-curve in Fig. 4(a) is caused by the fact that the OD data in the central (OD > 1) region was actually obtained from a Sinc^2 fit to the measured data, and this fit and the measured curve do not match exactly at the joining points at $|x/w| \sim 0.35$.

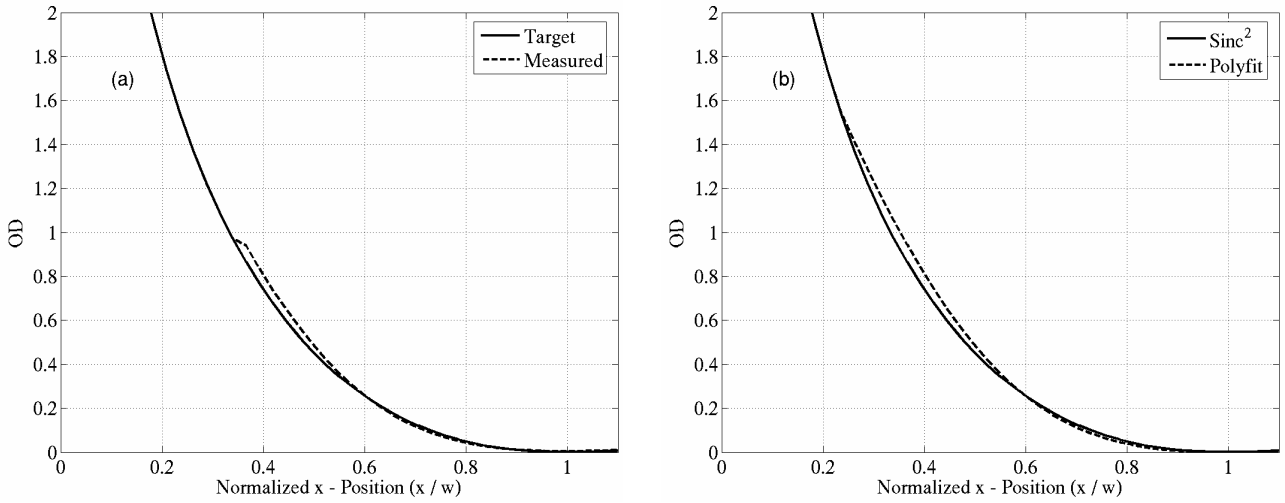

Figure 4. OD profiles of a linear-Sinc^2 occulting mask. (a) OD profile measured at λ=785nm versus a Sinc^2 target; (b) Same as part (a), except that the measured curve is replaced by a Sinc^2-curve in all regions except in the interval $0.2 < |x/w| \leq 1$, where the OD curve is represented by a 5th-order polynomial. The latter will be called "Polyfit"occulter in this paper. The occulter width parameter w = 144μm in all cases. The OD profile is an even function of x, so the other half of each profile is not shown.

After determining what in the occulting mask OD profile contributes to the contrast performance improvement of the HCIT, we constructed a new occulter OD profile. This new occulter has a Sinc^2 profile with w=144μm in all regions except in two intervals $0.2 < |x/w| \leq 1$, where the OD curve is represented by a 5th-order polynomial. The polynomial curve portion of this profile starts from $|x/w|=1$ and extends to $|x/w| \sim 0.2$ until it touches the Sinc^2 curve. It is shown with the dashed-curve in Fig. 4(b), and will be called "Polyfit" occulter to distinguish it from the standard Sinc^2 profile. Both the Sinc^2 and the Polyfit occulter masks will be used in this study.

3. RESULTS

A detailed and realistic optical model of the HCIT was set up by using its "as-built" prescription, and a speckle-nulling algorithm [1] was also implemented. This algorithm is identical in principle to what was implemented on the testbed, with some differences in the implementation detail. The fundamental principle of this algorithm was explained in Ref. 1 and will not be repeated here. In a typical speckle-nulling process on the testbed, the starlight image intensity is measured with the CCD science camera in the back focal plane, it is processed to obtain a new corrective phase map, the DM control setting is modified with this new information, and these iteration steps are repeated until the contrast reaches a desired value or the speckle-nulling process becomes ineffective. In our simulations, on the other hand, the final image plane intensity map is obtained by running MACOS with a given set of parameters. By carrying out end-to-end full diffractive propagation analysis with this optical model, we are not only able to evaluate the HCIT's performance under various different conditions, but also to simulate the speckle-nulling optimization process and make reasonable predictions on its capability in achieving our contrast target.

The DM used on the HCIT has 1024 (32x32) actuators arrayed on a 1mm pitch. It can produce a high-contrast half dark field in an area defined the by the controllable spatial frequency of the DM. The targeted high-contrast window in the HCIT coronagraph image is [xmin xmax ymin ymax] = [4 10 -10 10]*λ/D, with Mean Contrast, C_m, and Contrast at 4λ/D, C_4, as the ultimate metrics of the HCIT's performance. Here, the C_m is defined as the contrast value averaged over the window of [4 10 -10 10]*λ/D, and the C_4 as the one averaged over a smaller window of [4 5 -0.5 0.5]*λ/D. And the quantity Contrast is calculated using Eqn. 12 in Ref. 9, but without any averaging.

In our simulations, the speckle-nulling is carried out with the following steps: 1) Adjust the de-space distance of the occulting mask from its nominal position so that the total energy at the final focal plane (or the scattered light) is minimized (usually 0 ~ 2mm). 2) Carry out speckle-nulling for 5 iterations in the full right half-plane, for 5 iterations in the full left half-plane, and repeat these two sub-steps one more time. This step reduces the amount of light leaking through the Lyot Stop. 3) Continue the speckle-nulling in the full right half-plane for 100 iterations. In this case, the size of the speckle-nulling window is determined by the controllable spatial-frequency bandwidth of the DM. 4) Continue the speckle-nulling inside a reduced window [3 11 -11 11]*λ/D for several hundred iterations. 5) Conduct the rest of speckle-nulling iterations in an even smaller window of [3 10 -10 10]*λ/D. There is an additional parameter except the speckle-nulling window that is needed in the speckle-nulling algorithm, namely, the "gain factor" γ. It is used to scale the correcting phase map (or DM corrective surface pattern) obtained by processing the coronagraph image intensity. The right value for γ depends on the implementation details of the algorithm, and should be determined through numerical experimentation. The goal is to make the speckle-nulling process as efficient as possible. It should be pointed out that the MACOS-based speckle-nulling simulation process is fairly time-consuming. In our case, for a grid size of 512x512 and with an Intel Xeon 3.2GHz dual-processor workstation, it takes about two hours for 100 speckle-nulling iterations.

We calculate the broad-band contrast in the following way. We divide the full bandwidth Δλ=80nm into 8 equal segments with a wavelength increment δλ=10nm, representing the Δλ=80nm broad-band light with 9 narrow-band (or monochromatic) beams with equal intensity centered at λ_1 = 760nm, λ_2 = 770nm, …, λ_9 = 840nm, respectively. We calculate the final image plane intensity maps at each of these wavelengths separately, rescale them to the pixel size same as that of $\lambda_5 = \lambda_o$ = 800nm beam, and average them to obtain the broad-band image intensity map. We reduce the number of the images to average when calculating a broad-band image corresponding to a smaller bandwidth Δλ. For example, to calculate the broadband image corresponding to Δλ=20nm, we average the images at λ_4 = 790nm, λ_5 = 800nm and λ_6 =810nm only. We perform this calculation on the star and planet images separately to obtain their broadband images first, then use these averaged images to obtain a broadband contrast map.

In the following, we describe our modeling and simulation results in two different categories: One is ideal (phase-free) occulting mask, and the other is realistic (with parasitic phase) occulting mask.

3.1 Ideal occulting mask

First, we consider several ideal cases of the occulting mask to understand the contrast noise floor and the ultimate performance capability of the HCIT. An ideal occulting mask has a transmittance profile as shown by either curve in Fig. 4(b) with its phase-delay the same at all OD values. In this part of our simulations, we set the occulting mask phase to zero, and evaluated the following three cases: 1) The light source exhibits drooping as shown in Fig. 5 of Ref. 5, but all of the optics are free of phase errors ("No Zygo"). 2) The light source exhibits drooping, all of the optics have phase

errors as measured with the Zygo interferometer ("With Zygo", as shown in Fig. 4 of Ref. 5), and the occulter has a standard Sinc^2 OD profile. 3) Same as Case 2, except that the occulter has the "Polyfit" OD profile. The word "No Occ-Phase" in the figure legend indicates that the occulter phase is not included in this simulation. The detector noise is not taken into account in this paper.

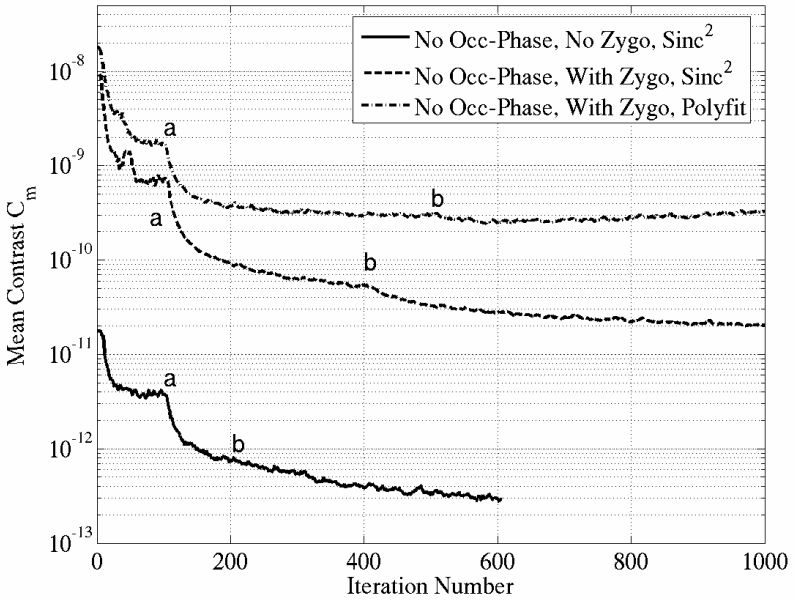

Figure 4. Mean Contrast C_m during the speckle-nullling process. Letter "a" indicates the point where the speckle-nulling window was reduced from the full right-half plane to [3 11 -11 11]*λ/D, and the letter "b" indicates the point where it was further reduced to [3 10 -10 10]*λ/D.

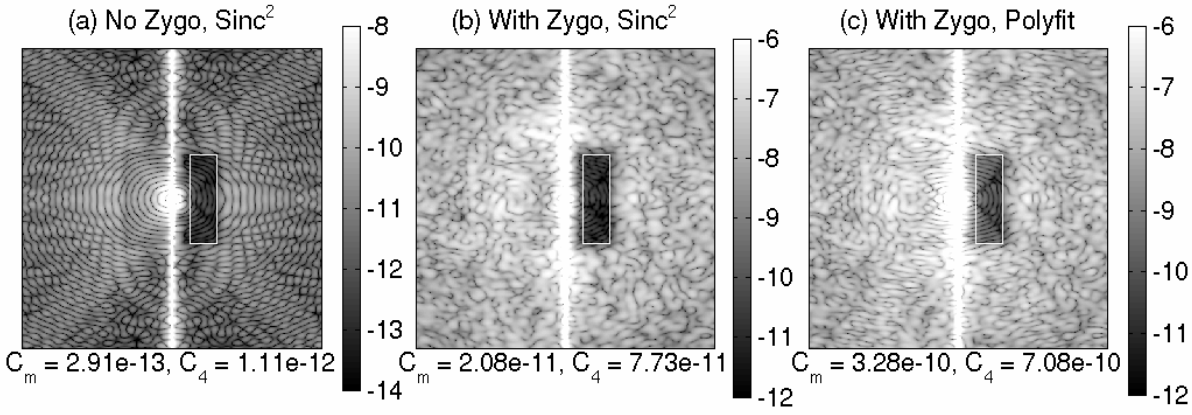

Figure 5. Log-scale contrast maps under three different conditions. The white-colored rectangular box in each graph indicates the field angle window corresponding to [4 10 -10 10]*λ/D. C_m shown as the x-label is the mean contrast inside the [4 10 -10 10]*λ/D box, and C_4 is the contrast at 4λ/D obtained by averaging the contrast values inside the smaller [4 5 -0.5 0.5]*λ/D box. (a) Do not including the phase errors for all optics, and with a Sinc^2 occulter. (b) Including the phase errors for all optics, and with a Sinc^2 occulter. (c) Including the phase errors for all optics, and with a Polyfit occulter.

Figure 4 displays the process of speckle-nulling in terms of the monochromatic Mean Contrast value C_m at λ_o = 800nm. In this figure, the letter "a" indicates the point where the speckle-nulling window was changed from the full right half-plane to [3 11 -11 11]*λ/D rectangle, and the letter "b" indicates the point where this window was further reduced to [3

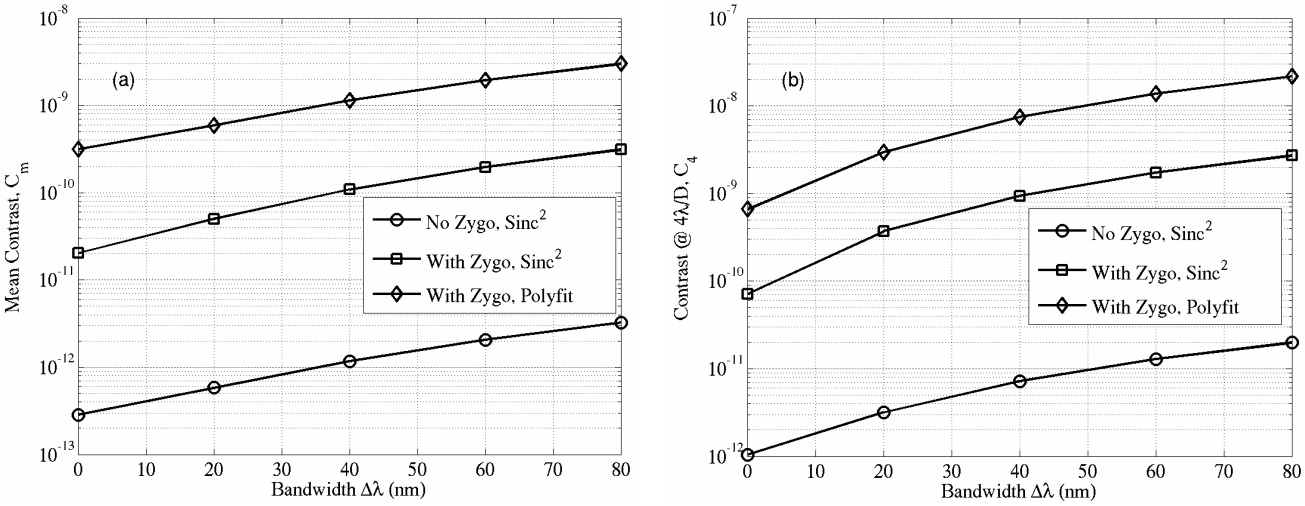

Figure 6. Broadband contrast as a function of bandwidth Δλ for the 3 cases shown in Figs. 4 and 5. (a) Mean contrast, C_m. (b) Contrast at 4λ/D, C_4..

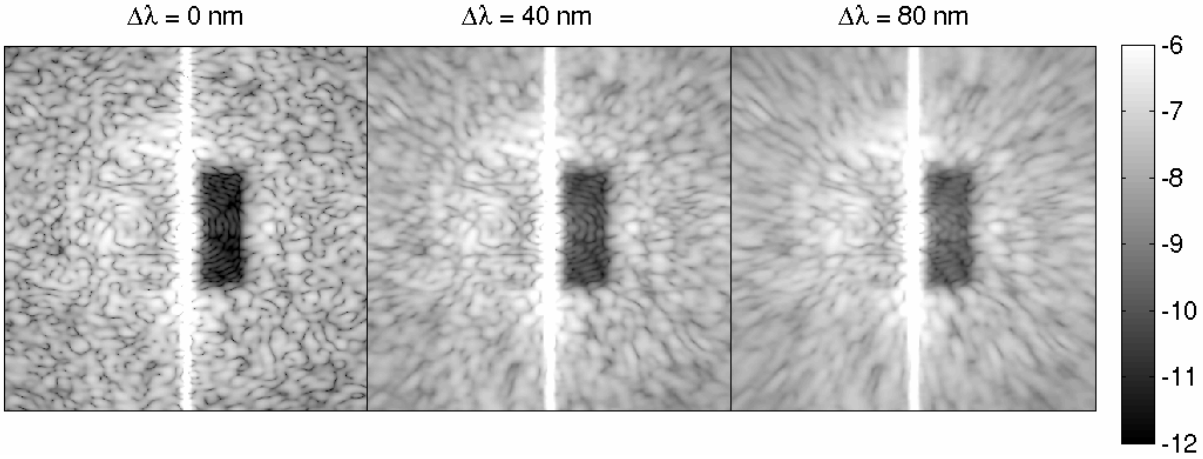

Figure 7. Log-scale contrast maps obtained for the case of (b), that is, with phase errors of all the optics and with a Sinc^2 occulter for Δλ=0 nm, 40 nm and 80 nm, respectively. The three contrast maps are plotted as one figure in the same scale to clearly visualize the difference among the 3 cases.

10 -10 10]*λ/D. Figure 5 shows the final results of the contrast map obtained for the above 3 cases. It has been shown in Ref. 5 that the HCIT optical model has a mean contrast noise floor of C_m ~$1x10^{-14}$ when the amplitude drooping caused by non-uniform illumination is not included. As we can see from Figs. 4-5, the amplitude drooping effect raises this floor to C_m~$2x10^{-11}$, but it can be improved to C_m=$2.9x10^{-13}$ by speckle-nulling for 600 iterations. That is, scattered light caused by the amplitude drooping of the source can be eliminated to certain degree through speckle-nulling. Here we stopped the speckle-nulling optimization after a total of 600 iterations because no much improvement is expected beyond that point. The intrinsic phase errors introduced by all of the optics into the optical system greatly degrade the contrast performance of the HCIT as expected. In this particular case, the mean contrast degrades from C_m~$2x10^{-11}$ to C_m>$1.0x10^{-8}$ just because of the phase errors of all the optics. We could have improved this contrast value to C_m=$2.1x10^{-11}$ after a total of 1000 speckle-nulling iterations, as shown in Figs. 4 and 5.

In order to understand how an ideal (phase-free, or band-limited) Polyfit occulter performs as compared to the standard Sinc^2 occulter, we repeated our speckle-nulling optimization process for the Polyfit occulter. The results are also shown

in Figs. 4 and 5. As we can see, when the occulter is phase-free, the standard Sinc^2 occulter performs much better, more than an order of magnitude in terms of C_m to be exact.

Figures 6(a) and 6(b) show the mean contrast, C_m, and the contrast at $4\lambda/D$, C_4, respectively, as a function of bandwidth $\Delta\lambda$ for the above 3 cases. Each curve was obtained with one DM correcting phase map that corresponds to the last iteration value in Fig. 4. That is, the DM correcting phase was optimized for the monochromatic wavelength operation of the HCIT optical system at λ_o =800nm, and it is used to evaluate the HCIT's performance at the increasingly broader bandwidth in Fig. 6. As we can see, each contrast value decreases (that is, the values of C_m and C_4 increase) by approximately an order of magnitude when the light bandwidth is increased from $\Delta\lambda$ =0nm (monochromatic beam) to $\Delta\lambda$ =80nm.

3.2 Realistic occulting mask

Next, we consider two cases of realistic occulting mask. Modeling and simulations in this subsection help us understand what behavior we can expect from the HCIT under various practical conditions. Figure 8 shows that when the occulting mask phase is present, the Polyfit occulter works better than the standard Sinc^2 occulter. This has been mentioned earlier in Sub-section 2.1, and the proof of that claim is given here in Fig. 8. It has been shown previously [5] that either one of the occulting mask parasitic phase and the phase errors of the HCIT optics result in a great degradation in the HCIT's contrast performance; and among these two factors, the phase errors of the occulting mask have stronger adverse effects. The results of the case of "With Zygo" and Sinc^2 occulter in Figs. 4 and 8 once again prove this point.

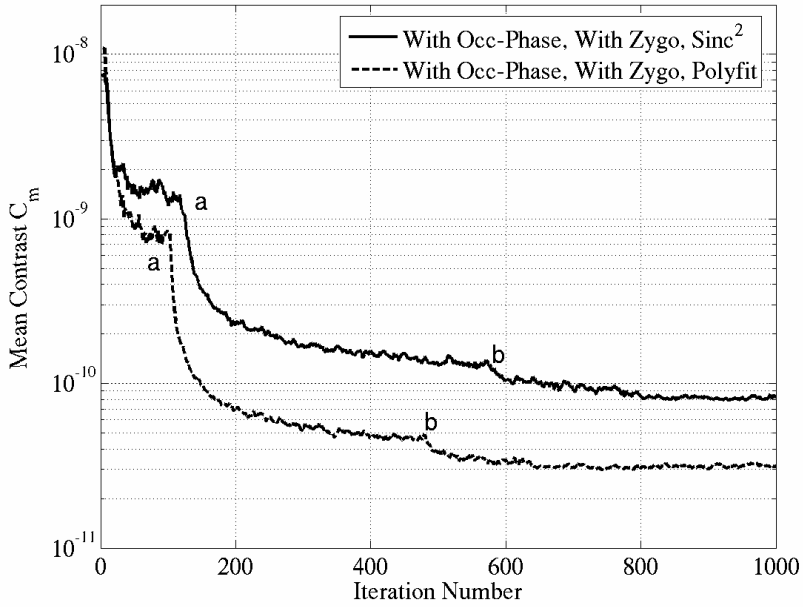

Figure 8. Mean Contrast C_m during the speckle-nullling process. Letter "a" indicates the point where the speckle-nulling window was reduced from the full right-half plane to [3 11 -11 11]*λ/D, and the letter "b" indicates the point where it was further reduced to [3 10 -10 10]*λ/D. *w*=144μm in both cases. The result for the Sinc^2 occulter was obtained with λ_o=785nm.

Figures 9(a) and 9(b) show C_m and C_4 as a function of bandwidth for the case of a Polyfit occulter. Three examples of contrast maps at three different bandwidth values and corresponding to the regular Polyfit occulter are given in Fig. 10. The occulter phase and the phases of all the optics are included in this simulation. In Figs. 9(a) and 9(b), the curves marked as "Broadband Polyfit Occulter" were obtained for an occulting mask that has a phase profile as shown in Fig. 3(b) but that phase profile does not change with wavelength. Such a characteristic is typical for an occulter which is broadband in terms of its phase delay. As we can see, making the occulter broadband improves the C_m by a factor of ~4 and the C_4 by a factor of ~2 when $\Delta\lambda$ = 80nm under the current optical system condition. This simulation predicts that the best results obtainable with the current occulting mask and the current DM setting (or correcting phase) is C_m = $1.1\text{x}10^{-8}$ and C_4 = $4.9\text{x}10^{-8}$, respectively. This result does not meet the requirement of this project's current milestone.

However, it must be pointed out that the occulting mask and the Lyot Stop used in this study are the same as before and have not been optimized for a broadband operation. Also, a broadband speckle-nulling algorithm has not been developed or implemented in the current optical simulation tool. We will optimize the occulter and the Lyot Stop as well as the speckle-nulling algorithm for broadband operation as a continuation of this study and expect such optimizations will improve the HCIT's performance to a satisfactory level.

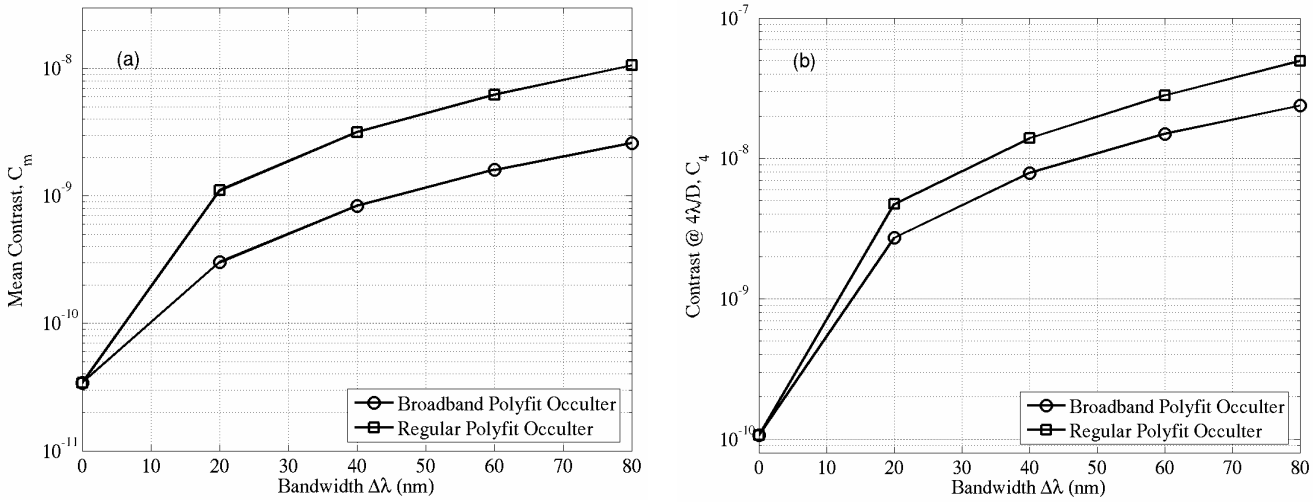

Figure 9. Broadband contrast as a function of bandwidth Δλ for the cases of a broadband and a regular occulting masks. .The broadband occulter has a phase profile as shown in Fig. 3(b), but such a phase profile does not change with wavelength. (a) Mean contrast, C_m. (b) Contrast at 4λ/D, C_4.

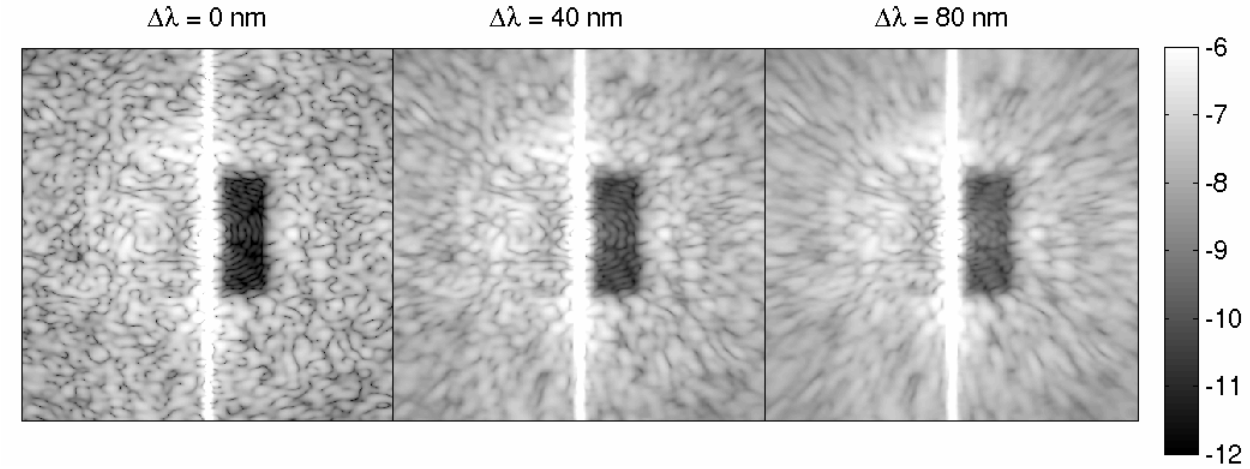

Figure 10. Log-scale contrast maps obtained for the case of a regular Polyfit occulter for Δλ=0 nm, 40 nm and 80 nm, respectively. The three contrast maps are plotted as one figure in the same scale to clearly visualize the difference among the 3 cases.

4. CONCLUSION

We have continued our examination of the cause of the improved performance of a measured occulting mask OD profile, and conducted a preliminary investigation on the broadband wavelength behavior of JPL's high-contrast imaging testbed (HCIT) through optical modeling and simulations. By examining both the ideal and realistic cases of occulting masks as

well as the HCIT's other optical components, we have found the following about the fabricated occulting mask and the contrast performance of the HCIT: 1) The slightly wider, non-$Sinc^2$ central peak of the measured occulting mask's OD profile is responsible for the improved contrast performance of the HCIT. 2) Under the realistic amplitude drooping condition of the illuminating light source, an ideal or band-limited linear-$Sinc^2$ occulting mask and error-free optics result in $C_m=3.2x10^{-12}$ (mean contrast) and $C_4=2.0x10^{-11}$ (contrast at $4\lambda/D$), respectively, when an illuminating beam with a central wavelength $\lambda_o=800nm$ and bandwidth $\Delta\lambda=80nm$ is used. However, when the phase errors of the HCIT optics are included, these results degrade to $C_m=3.1x10^{-10}$ and $C_4=2.7x10^{-9}$, respectively. 3) When a realistic occulting mask having parasitic phase-shift errors (or non-band-limited occulting mask) is used, the obtainable contrast values for $\lambda_o=800nm$ and $\Delta\lambda=80nm$ further reduce to $C_m=1.1x10^{-8}$ and $C_4=4.9x10^{-8}$, respectively, under the current condition of the HCIT's optical system and with a DM correcting phase map obtained through monochromatic speckle-nulling optimization. We will continue this work to improve the above broadband performance of the HCIT by optimizing the occulting mask and Lyot Stop parameters for broadband operation and by developing and implementing a broadband speckle-nulling algorithm in our optical analysis tool.

ACKNOWLEDGEMENTS

This work was performed at the Jet Propulsion Laboratory, California Institute of Technology, under a contract with the National Aeronautics and Space Administration. The authors acknowledge helpful discussion with Dwight Moody, Brian D. Kern, and Daniel Wilson.

REFERENCES

1. John T. Trauger, Chris Burrows, Brian Gordon, Joseph J. Green, Andrew E. Lowman, Dwight Moody, Albert F. Niessner, Fang Shi, and Daniel Wilson, "Coronagraph contrast demonstrations with the high-contrast imaging testbed," Proc. SPIE, **5487**, 1330, 2004.
2. Andrew E. Lowman, John T. Trauger, Brian Gordon, Joseph J. Green, Dwight Moody, Albert F. Niessner, and Fang Shi, "High-contrast imaging testbed for the Terrestrial Planet Finder coronagraph," Proc. SPIE, **5487**, 1246, 2004.
3. Scott A. Basinger, and David C. Redding, "Terrestrial Planet Finder coronagraph optical modeling," Proc. SPIE, **5528**, 1, 2004.
4. *Modeling and Analysis for Controlled Optical Systems User's Manual*, Jet Propulsion Laboratory, California Institute of Technology, Pasadena, CA.
5. Erkin Sidick, Fang Shi, Scott Basinger, Dwight Moody, Andrew E. Lowman, Andreas C. Kuhnert, and John T. Trauger, "Performance of TPF's High-Contrast Imaging Testbed: Modeling and simulations, "Proc. SPIE, **6265**, 62653L, 2006.
6. Daniel W. Wilson, Paul D. Maker, John T. Trauger, and Tony B. Hull, "Eclipse apodization: realization of occulting spots and Lyot masks," Proc. SPIE, **4860**, 361, 2003.
7. M. Kuchner and W. Traub, "A coronagraph with a band-limited mask for finding terrestrial planets," *Astrophys. J*., **570**, 900, 2002.
8. Peter G. Halverson, Micheal Z. Ftaclas, Kunjithapatham Balasubramanian, Daniel J. Hoppe, and Daniel W. Wilson, "Measurement of wavefront phase delay and optical density in apodized coronagraphic mask materials," Proc. SPIE, **5905**, 59051I, 2005.
9. Joseph J. Green and Stuart B. Shaklan, "Optimizing coronagraph designs to minimize their contrast sensitivity to low-order optical aberrations," Proc. SPIE, **5170**, 25, 2003.